Global NEST Journal, Vol 27, No 2, 06875

Cadmium-modified zeolite (LTA, GIS, FAU) for isopropanol adsorption and photocatalytic degradation

Nguyen Thi Truc Phuong[1,2], Nguyen Tri Thong[1,2], Lam Tien Thuan[1,2], Ngo Tran Hoang Duong[1,2] and Nguyen Quang Long[1,2]*

[1]Faculty of Chemical Engineering, Ho Chi Minh City University of Technology (HCMUT), 268 Ly Thuong Kiet Street, District 10, Ho Chi Minh City, Vietnam

[2]Vietnam National University Ho Chi Minh City, Linh Trung Ward, Thu Duc City, Ho Chi Minh City, Vietnam

Received: 08/10/2024, Accepted: 09/12/2024, Available online: 13/12/2024

*to whom all correspondence should be addressed: e-mail: nqlong@hcmut.edu.vn

https://doi.org/10.30955/gnj.06875

Graphical abstract

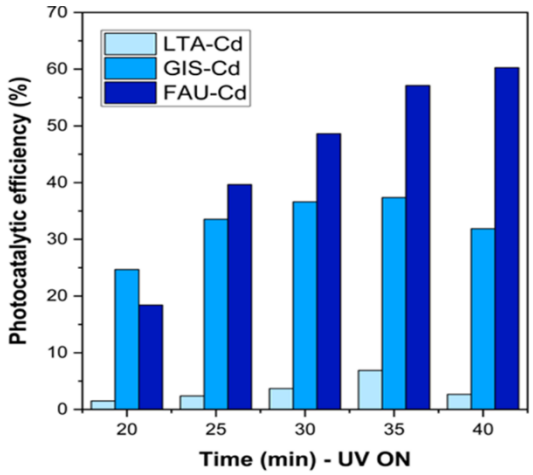

Abstract

In this study, various types of zeolite support (LTA, GIS-NaP1, and FAU-type Y) were coupled with CdO active sites to develop effective photocatalysts for volatile organic compounds (VOC) treatment (isopropanol as a model). Notably, both LTA-Cd and FAU-Cd samples retained the structure of the original zeolite, as indicated by the presence of characteristic peaks in their X-ray diffraction (XRD) patterns, whereas the transformation was seen in GIS-Cd sample. Cadmium oxide formation and distribution on the catalyst's surface were confirmed through XRD analysis, scanning electron microscopy (SEM) images, and three-point energy-dispersive X-ray spectroscopy (EDX) mapping. When comparing the efficacy in treating isopropyl alcohol (IPA) among the samples, FAU-Cd exhibited the best performance, containing only 1.59% of cadmium element. Interestingly, the variation in moisture stream ratio had minimal impact on IPA adsorption capacity, and its effect on the photocatalytic activity of the FAU-Cd sample could be negligible. It suggests that FAU-Cd holds promise as an effective photocatalyst for environmental cleanup purposes.

Keywords: photocatalyst, IPA degradation, catalyst based on zeolite, VOCs

1. Introduction

Nowadays, environment is on its way becoming the key issue of the world. Adding on to this point, the VOCs (volatile organic compounds) contamination is one of biggest motives leading to these effects, and 2-propanol (IPA) is such an instance owing to its utilization throughout the COVID 19 epidemic (Cimolai, 2020). IPA can be found in numerous industrial merchandises as sanitizers, household products and rubbing alcohol (Wiegand, 2024). As a toxic alcohol, isopropanol ingestion not only can cause clinical intoxication, but also may profound obtundation (Co & Gunnerson, 2019). Hence, it is vitally crucial to have an IPA treatment step before discharging it into the environment. There are numerous different methods for IPA treatment purpose, such as adsorption (Liu *et al.* 2019), absorption (Gao *et al.* 2023), membrane separation (Dmitrenko *et al.* 2022), catalytic oxidation (Guo *et al.* 2022), and photocatalysis method (Tan *et al.* 2019). Instead of facing many issues in the selection of absorbent and the optimisation of adsorption equipment, same as with others methods's difficulties (Gao *et al.* 2023), the photocatalysis method prove it is one of the most advanced method for its great beneficial in eliminating IPA due to takes placing of photocatalytic reaction at atmospheric condition, with the ability of using sunlight and easy in designing reactor (Almaie *et al.* 2022). In photocatalysis method, H^+ and electron are separated and then react with O_2 and OH^-, forming the active $^{\bullet}O^{2-}$ and $^{\bullet}OH$ (Wu *et al.* 2021).

$$\text{Catalyst} + hv \rightarrow h^+ + e^- \quad (1)$$

$$O_2 + e^- \rightarrow \cdot O_2^- \quad (2)$$

$$H_2O + h^+ \rightarrow \cdot OH + H^+ \quad (3)$$

$$O_2^- + H^+ \rightarrow HO_2 \quad (4)$$

$$HO_2 \rightarrow O_2 + H_2O_2 \quad (5)$$

$$HO_2 + H_2O + e^- \rightarrow H_2O_2 + OH^- \quad (6)$$

$$OH + OH \rightarrow H_2O_2 \quad (7)$$

$$H_2O_2 + e^- \rightarrow OH + OH^- \quad (8)$$

The widely accepted photocatalytic oxidation (PCO) model (Enesca & Cazan, 2020) suggests that electrons and holes typically distribute to the surface of photocatalysts where they engage in reactions with VOCs. Nonetheless, an alternative path involves electrons and holes recombining before they can effectively decompose VOCs, thereby compromising the efficiency of VOC decomposition. When photo-generated electrons and holes diffuse to the surface without recombining, these electrons and activated holes (h^+) account for catalyzing redox reactions with VOCs adsorbed on the photocatalyst surface (Mo *et al.* 2009). The electrons produced by photocatalysts could counter with electron acceptors like O_2 (Equation (2)), while the holes can oxidize electron donors such as H_2O, initiating the generation of radicals (Equation (3)). These radicals (·OH), when released from the photocatalyst surface, trigger the formation of reactive oxygen species (ROS) (Equations (2)–(8)), which also react with VOCs due to their unsaturated bonds. Common radicals and ROS include ·OH, $\cdot O^{2-}$, HO_2, and H_2O_2. Ultimately, they oxidize VOCs into CO_2, H_2O, and other byproducts.

Metal oxides have long had applications such as photocatalytic applications for environmental remediation, decarbonization, and energy sustainability (Danish *et al.* 2020). Previous studies by Takashi *et al.* investigated the improvement of photocatalytic efficiency in TiO_2-zeolite composites aimed at enhancing the photodegradation of 2-propanol in water (Kamegawa *et al.* 2013). Zhang and colleagues synthesized a photocatalyst combining TiO_2/acid leaching zeolite, demonstrating enhanced performance in removing various organic pollutants (G. Zhang *et al.* 2018). Regrettably, TiO_2-based photocatalysts possess a wide band gap (~3.2 eV), making them suitable only for UV radiation absorption, which constitutes approximately 5% of solar energy. Additionally, they exhibit a short lifetime of photoexcited charge carriers (X. Yan *et al.* 2017), (Ong *et al.* 2014), (Y. Yan *et al.* 2014). Besides, CdO exhibits excellent conductivity and enhanced chemical stability as a result of a higher carrier concentration resulting from oxygen vacancies or interstitial states of cadmium (Rana *et al.* 2019). CdO features superior electron mobility and absorbs visible radiation effectively, making it highly suitable for photocatalytic applications (Rajput *et al.* 2018). In particular, cadmium oxides has many diverse applications such as solar cells, catalysis, chemical and gas sensors, phototransistors and photodiodes; and is also chosen as a photocatalyst due to its band gap is 2.3 eV, suitable for light with wavelengths ranging from 500 nm or less (Mohammed *et al.* n.d.). In the study of Kurugundla Gopi Krishna and colleagues, CdO in a ZnO/CdO nanocomposite was used as a sensor for BTX (benzene, toluene, styrene), resulting in this sensor being a time-honored material with quick response and recovery times (Krishna *et al.* 2024). Therefore, CdO has potential to treat IPA with the energy provided by UVA - 352nm light.

Metal oxides are not often used alone because in their non-porous form they only interact with molecules at the surface and are not used with internal molecules so they must be accompanied by a by a support (Mabate *et al.* 2023). Among the various adsorbent supports for photocatalysts, zeolite - a porous material with a 3D network structure, has been identified as the most promising candidate (Moshoeshoe *et al.* 2017). Zeolites are commonly used adsorbents because of their exceptional micropores, cavities, and channels. With pore diameters between 5 and 20 Å, they are ideal for adsorbing a variety of VOC molecules (K. P. Veerapandian *et al.* 2019). Zeolite has advantages such as large surface area, thermal stability, environmental friendliness, abundant acid/base sites that can minimize the electron-hole pairs recombination, adjustable surface property, etc (Hu *et al.* 2021). Conventional zeolite is an aluminosilicate-type microporous material made of tetrahedral SiO_4 and AlO_4 units. Each AlO_4 tetrahedron introduces a net negative charge, which needs to be compensated by additional exchangeable cations (such as H^+, Na^+, K^+, Ca^{2+}, Mg^{2+}, and others). These cations are loosely held and can be easily exchanged under mild conditions (Hu *et al.* 2021), in particular, the high ability to exchange ions with other metals makes carrying metal ions to the surface much easier than with other carriers (Belviso, 2020).

This study synthesized Cd-exchange zeolites as photocatalysts with a simple procedure for IPA treatment in the continuous gas. With a high specific surface area, fine porous, and stability, different zeolites (GIS-NaP1, FAU, and LTA) become promising supporters to enhance IPA adsorption capacity. Besides, zeolite supporters can decrease the fast recombination of electrons and holes with CdO active sites, increasing the usability of the photocatalysts. In addition, the IPA treatment ability in the humid environment was also investigated for enhanced application.

2. Experimental

In this study, three types of zeolite were applied for preparing the photocatalyst. Zeolite GIS (Na-P1) was prepared based on published procedure (Sharma *et al.* 2016); zeolite LTA was obtained from Chau-Thinh-Phat Co. and zeolite FAU (type Y) was prepared based on published procedure (Robson, 2001), (Tu *et al.* 2019). Each zeolitic material were exchanged with ion Cd^{2+} by stirring 1.0 g zeolite in 50 mL of 500 ppm $Cd(NO_3)_2$ solution for 24 hours at room temperature. After filtration the obtained solid was washed and dried at 80 ℃ overnight. Afterwards, it was calcined at 400 ℃ for 2 hours to form the Cd-exchanged zeolite photocatalysts. Crystallization of all the samples were investigate with X-ray diffraction analysis using D8 Advance, Bruker. Nitrogen physisorption was conducted at -196 ℃ with Nova 2200e Quantachrome after vacuuming samples at 300 ℃ for 2 hours. The morphological features of prepared membranes were determined using a scanning electron microscope (Hitachi S4800).

IPA photodegradation was investigated with a photocatalytic annular reactor (Nhan *et al.* 2024) including

an outer quartz tube (35 mm of outside diameter and 1mm of thickness) connected to the gas tubes at both ends, an inner glass tube (25 mm of outside diameter and 1 mm of thickness) sealed at both ends and a light emitting system of four UVA-lamps (Sankyo Denki F10T8BLB, Japan) with 352 nm of wavelength and 1.5W of emission capacity that symmetrically located 2.5 cm far from reactor. In preparation step, 0.2 g of catalyst sample was dispersed in alcohol solution (98%) with ultrasonic for 10 minutes to make the fine suspension before being coated on the surface of the inner tube of the reactor by the spin spray coating method. The catalytic coated tube was then calcined at 300 ℃ for 2 hours before all experimental tests. The nitrogen gas stream carries IPA by bubbling method, then mixed with oxygen, nitrogen, and moisture if available to form the IPA input gas stream with a determined concentration before passing through the sample. In this study, the input concentration of IPA is fixed at about 1200 ppmv. A needle valve controlled each flow and monitored using a flow meter. The mixing chamber was used to stabilize the concentration of the inlet gas stream. The output gas flow is analyzed directly by GC-FID equipment. IPA absorbed capacity (mmol/g) and IPA photocatalytic efficiency (%) was calculated with (1), and (2) formulas:

$$q\left[\frac{\text{mmol}}{\text{gcat}}\right]=\frac{P\times F}{R\times T}\times\frac{1}{m_{\text{cat}}}\times\left(1-\frac{C_i}{C_0}\right)*1000 \quad (1)$$

$$X(\%)=\left(1-\frac{C_i}{C_0}\right)*100 \quad (2)$$

where q is the saturated adsorption capacity (mmol/g), P is the pressure of IPA (atm), F is the total gas flow (ml/min), T is the temperature of IPA gas mixture (K), R is the gas constant (L.atm.K^{-1}.mol^{-1}), C_0 is the inlet concentration of the adsorbed gas (ppmv) and C_i is the outlet concentration of the adsorbed gas (ppmv).

3. Results and dicussions

XRD patterns of all samples were expressed in Figure 1, along with the standard peaks of CdO (JCPDS 05-0640), zeolite LTA (JCPDS 01-078-2452), no zeolite FAU (JCPDS 01-077-029), and zeolite GIS-NaP1 (JCPDS 00-039-0219). The characteristic peaks of CdO at 2θ = 33° was observed in all the ion-exchanged zeolite samples, which proved the CdO crystallization after these modifications. The characteristic peaks of FAU zeolite (2θ = 6.1°, 10°, 11.8°, 15.5°, 18.5°, 20.1°, 23.6°, 27.4°, and 29.3°, respectively), and LTA zeolite (2θ = 7.2°, 10.3°, 12.6°, 16.2°, 21.8°, 24.0°, 27.2°, 29.9° and 34.2°, respectively) appeared in FAU-Cd and LTA-Cd sample, have shown the stable of zeolite frameworks after being modified in this study. In the GIS-Cd sample, the FAU framework's characteristic peak appearance is beside some standard peaks of GIS-NaP1 zeolite (2θ = 12.5°, 17.8°, 21.6°, 28.2°, 33.4°), which may come from the structural transformation of ion exchange combined with the thermal treatment method. Thus, there are the remain in structure of FAU and LTA zeolites sample after modifying with a well crystalline, while the opposite is true of GIS zeolites, where the process of exchanging Cadmium ion adversely effects the framework of zeolites. However, the CdO can be seen clearly on all samples, proving the successfully coating process of oxides on the surface of zeolites.

Nitrogen physisorption results of all samples are shown in Figure 2 and Table 1. The nitrogen adsorption-desorption curves have the shape of type I isotherms (Thommes *et al.* 2015), characterizing microporous materials - the basic properties of the zeolite framework. According to Table 1, the samples with cadmium have a smaller surface area than the initial zeolite (525.6 m^2/g of FAU-Cd < 588.2 m^2/g of FAU, 147.0 m^2/g of GIS-Cd < 194.8 m^2/g of GIS), which is suitable with the cadmium molecules have fulfilled a part of the zeolite pores. GIS-Cd and LTA-Cd have a smaller BET surface area than the FAU-Cd sample because the frameworks of GIS and LTA contain tiny micropores (ultramicro pores < 0.7 nm), which are difficult for nitrogen (Sayehi *et al.* 2020).

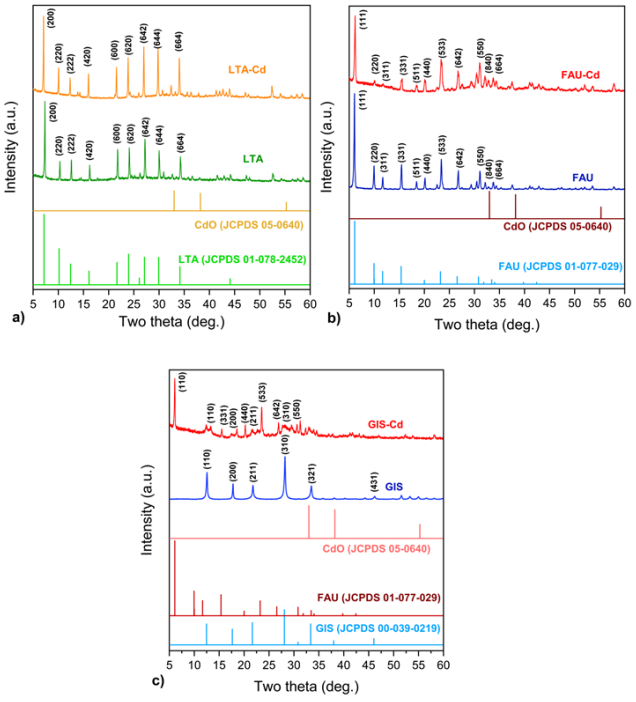

Figure 1. XRD patterns of cadmium exchanged zeolite: LTA-Cd **(a)**, FAU-Cd **(b)**, and GIS-Cd **(c)**

Table 1. Nitrogen physisorption parameters of all samples

Samples *Unit*	S_{BET} m^2/g	$S_{langmuir}$ m^2/g	$S_{external}$ m^2/g	V_{total} cc/g	V_{micro} cc/g
FAU	588.2	858.4	33.55	0.3325	0.2857
FAU-Cd	525.6	766.8	19.79	0.2957	0.2607
GIS	194.8	287.9	27.76	0.1291	0.0868
GIS-Cd	147.0	213.9	15.56	0.09662	0.0674
LTA	16.55	24.63	9.826	0.0609	0.0034
LTA-Cd	9.821	16.51	9.821	0.0190	0.0070

Turning to the SEM-EDX results of FAU-Cd samples, which were showed in Figure 3. The morphology of FAU zeolite can be observed at different resolutions of SEM images (Figure 3a, b, c), which are shape of octahedral crystalline, some are closer with the spherical particles with the diameter around 1µm. The similar morphology and particle size were also seen in the study of Danial for FAU zeolites (Aguilar Ramírez *et al.* 2021), proving the well-defined shape of zeolite still remaining after modification steps. Moving to the Cadmium distribution on the surface of zeolites, the EDX was conducted to reveal the elemental mapping of Cd. When mapping three points in the surface of the FAU-Cd sample (Figure 3d, e, f), the red dots indicate the uniform distributions of cadmium even in any area. The values of the cadmium element percentage are very similar at these different three points (1.68%, 1.61% and 1.49%, respectively), which are averagely about 1.59 %, meaning the relatively low content of active sites.

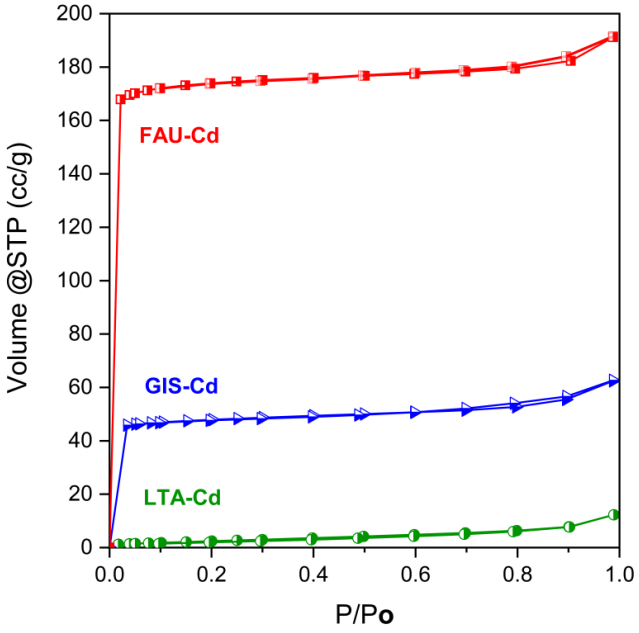

Figure 2. Nitrogen physisorption isotherms of Cadmium-exchanged zeolite samples

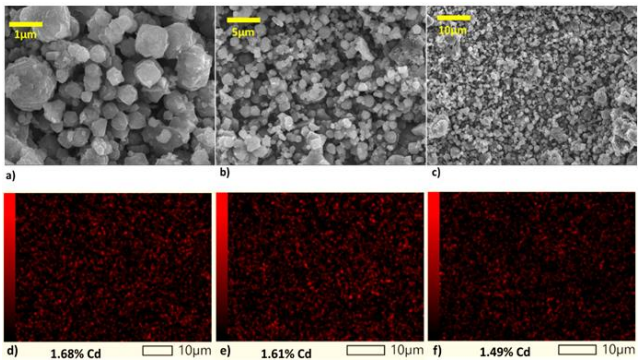

Figure 3. a, b, c) SEM images at different resolutions (x10000, x5000, x1000) of FAU-Cd sample; **d, e, f)** Cadmium element distribution of mapping three points in FAU-Cd 's surface

IPA removal between the ion-exchanged zeolite samples is in comparison in Figure 3a) and Figure 4 expresses the IPA adsorption processes of LTA-Cd, GIS-Cd, and FAU-Cd samples. Figure 3a is the IPA adsorption data following times in minutes, and Figure 3b is a capacity adsorption comparison. While the GIS-Cd and FAU-Cd sample has a close adsorption ability (near-coincident adsorption curves), the LTA-Cd is the worst with an adsorbed capacity of only 0.11 mmol/g, and the rapid equilibrium after 15 minutes. This can be because the pore size of the initial LTA is around 4Å (García-Soto *et al.* 2013), which is much smaller than the FAU zeolite pores of 7.5 Å (Ferreira *et al.* 2022). Thus, after being occupied by cadmium ions, the zeolite pores become smaller in size and lead to the IPA adsorption lessening. Adding on to the same above explanation, the IPA adsorption of GIS-Cd should be the smallest one with only 3.5Å of GIS-NaP1 pore size. However, after cadmium exchange and 400°C of calcination, the GIS-Cd sample has some characteristic peaks of the FAU framework (Figure 1c), claiming its FAU structure transformation and higher IPA degradation.

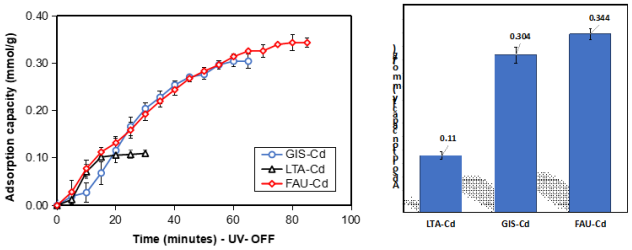

Figure 4. a) IPA adsorption follows time **b)** IPA adsorbed capacity comparison between different types of zeolite-exchanged cadmium

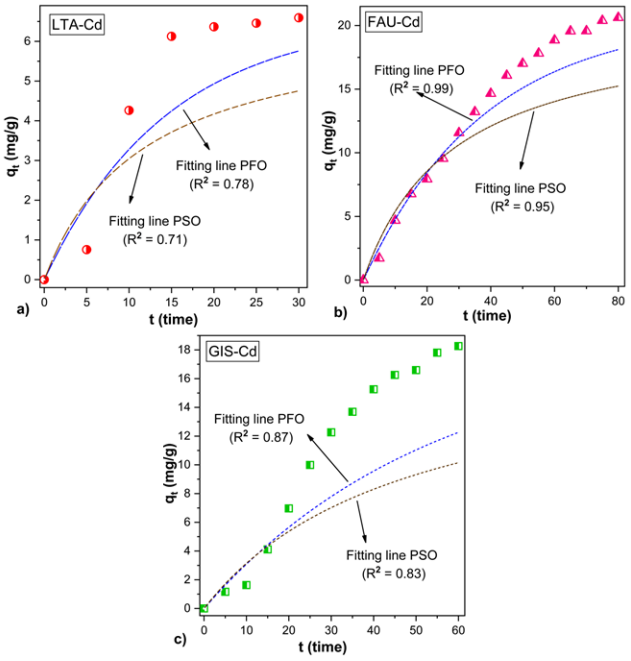

Figure 5. Fitting line of the sample: LTA-Cd **(a)**, FAU-Cd **(b)**, GIS-Cd **(c)** with Pseudo-first-order model and Pseudo-second-order model

Pseudo-first order (PFO) and pseudo-second order (PSO) are the most popular models for kinetic adsorption studies (J. Zhang, 2019). The differential form and integrating form of PFO model are described by the above equation (3), (4) (Wang & Guo, 2020):

$$\frac{dqt}{dt} = k_1(q_e - q_t) \quad (3)$$

$$\text{For the conditions of } q_0 = 0 : q_t = q_e\left(1 - e^{-k_1 t}\right) \quad (4)$$

The differential form and integrating form of PSO model are described by the above equation (5), (6) (Wang & Guo, 2020):

$$\frac{dqt}{dt} = k_1(q_e - q_t)^2 \quad (5)$$

$$q_t = \frac{q_e^2 k_2 t}{1 + q_e k_2 t} \quad (6)$$

In which, k_1 (1/min), k_2 (g/mg.min) are the rate constants of the PFO and PSO equations, respectively; q_e (mg/g) and q_t (mg/g) are the amounts of adsorbate uptake per mass of adsorbent at equilibrium and at any time t (min).

Table 1. Parameters of PFO and PSO fitting models of the samples.

Sample	PFO			PSO		
	q_e *(mg/g)*	k_1 *(1/min)*	R^2	q_e *(mg/g)*	k_2 *(g/mg.min)*	R^2
LTA-Cd	6.595	0.069	0.77	6.595	0.013	0.71
FAU-Cd	20.62	0.026	0.99	20.62	0.002	0.95
GIS-Cd	18.27	0.019	0.87	18.27	0.001	0.83

While the linear regression method is widely used for calculating the model parameters, owing to its simplicity, the nonlinear can provide consistent and accurate estimations for model parameters (Wang & Guo, 2020). Figure 5 and Table 2 show the fitting level of experimental data for the adsorption process to the PFO and PSO model through the nonlinear curve fit function of OriginLab with the integrating form of the models. According to the correlation coefficient value (R^2), the experimental data fits better with the PFO than the PSO model. In which, the reliability of the FAU-Cd sample to the PFO model is most with R^2 up to 0.99. The rate constant (k_1) of the LTA-Cd sample is high (0.069 1/min) because its adsorption process only happens with the outside surface, leading to the fast balance with low capacity (q_e only 6.595 mg/g).

Photo-catalytic results of all samples were expressed in Figure 7. With the close IPA adsorption capacity, turning the UVA light on, IPA photo-degradation of the GIS-Cd sample is 37.3% and 31.8% after 35 and 40 minutes, clearly smaller than FAU-Cd (57.1% at 35 minutes and 60.1% at 40 minutes), maybe because the cadmium exchange with FAU is more priority with larger pore size. Moreover, the above pore size difference of various zeolites makes the small number of cadmium molecules exchanged with LTA, resulting in a smaller photocatalytic efficiency (< 10% of photocatalytic efficiency at all time investigation). In summary, the FAU-Cd sample is the best one with the high IPA adsorption capacity and highest in photodegradation efficiency among them. The decrease in reaction efficiency over time when using LTA and GIS supporters may be attributed to prolonged irradiation, as photocatalytic processes at the gas-solid interface frequently exhibit a gradual decline in activity. According to Jaison's review (Jaison *et al.* 2023), this phenomenon arises from the formation of intermediates on the catalyst surface during VOC oxidation, which tend to interact more strongly with the catalyst than the initial reactants or become adsorbed onto the surface. The accumulation of these intermediates can obstruct photon absorption, thereby inhibiting the reaction. As an example, research by Einaga *et al.* further highlights that the efficiency of VOC removal experiences a sharp decline following two hours of photoirradiation involving organic compounds like toluene, benzene, cyclohexene, and cyclohexane (Einaga *et al.* 2002).

Moisture is one of the essential parameters impacting the adsorption process because it can inhibit the IPA molecules from contact with the zeolite surface. This issue is receiving more and more attention in a highly humid surrounding environment like Vietnam, especially when it is applied on an industrial scale. With the highest performance on the removal of IPA and IPA adsorption capacity (Figure 4 and Figure 7a), the FAU-Cd sample is used for these experiments with humid parameters. The IPA degraded investigations of the FAU-Cd sample with different moisture stream ratios (using three circumstances of 0%, 30%, and 60% relative moisture) were expressed in Figure 6 and Figure 7b. While IPA adsorption ability is nearly the same at different moisture conditions (about 0.35 mmol/g), the IPA photocatalytic process gives more deviation. The higher the moisture stream ratio is, the higher photocatalytic performance decreases. However, this downward trend is not significant (60.2%, 47.0%, and 35.5% after 40 minutes for FAU-Cd, FAU-Cd30, and FAU-Cd60, respectively), and the reason may come from the competition of free radicals supporting the reaction. The other study should focus on this phenomenon to get deeper insights into this research.

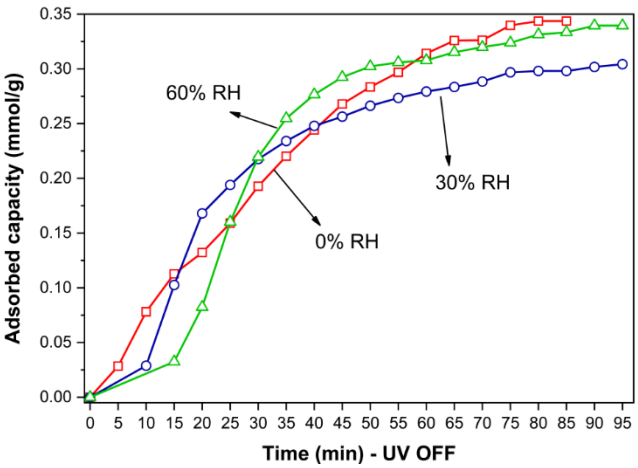

Figure 6. IPA adsorption capacity follows times with different moistures

4. Conclusion

This study successfully synthesized the photocatalysts based on different types of zeolite supporters (LTA, GIS-NaP1, and FAU-type Y) with the CdO active site by ion

exchanging method. The LTA-Cd and FAU-Cd samples still keep the framework of the initial zeolite when all characteristic peaks appear on their XRD patterns, while the GIS-Cd has a tendency to transform the supporter into the FAU structure. The CdO formation and distribution also have been indicated with XRD analysis and three-point EDX mapping. The comparison of IPA treatment ability between all samples shows FAU-Cd is the best one with only 1.59% of cadmium element, nevertheless, it had highest in IPA adsorption capacity and photocatalytic efficiency. Besides, the moisture stream ratio has almost no effect on IPA adsorption capacity while insignificantly affecting photocatalytic activity at the FAU-Cd sample.

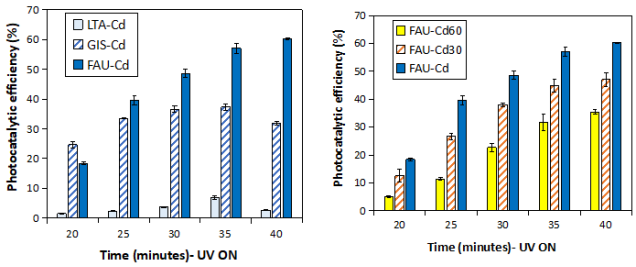

Figure 7. IPA photo-removal efficiency of **a)** different zeolite exchanged cadmium samples, **b)** FAU-Cd sample with different moisture ratio

Funding and declaration of competing interest

The authors declare that they have no known competing financial interests or personal relationships that could have appeared to influence the work reported in this paper.

Acknowledgments

This research is funded by Vietnam National University Ho Chi Minh City (VNU-HCM) under grant number: 562-2023-20-05. We also acknowledge HCMUT for supporting this research.

Data availability statement

The authors confirm that the data supporting the findings of this study are available within the article

References

Almaie, S., Vatanpour, V., Rasoulifard, M. H. and Koyuncu, I. (2022). Volatile organic compounds (VOCs) removal by photocatalysts: A review. *Chemosphere*, *306*, 135655. https://doi.org/10.1016/j.chemosphere.2022.135655

Belviso, C. (2020). Zeolite for Potential Toxic Metal Uptake from Contaminated Soil: A Brief Review. *Processes*, *8*(7), Article 7. https://doi.org/10.3390/pr8070820

Cimolai, N. (2020). Environmental and decontamination issues for human coronaviruses and their potential surrogates. *Journal of Medical Virology*, *92*(11), 2498–2510. https://doi.org/10.1002/jmv.26170

Co, I. N. and Gunnerson, K. J. (2019). Chapter 71—Iatrogenic and Poison-Derived Acid Base Disorders. In C. Ronco, R. Bellomo, J. A. Kellum. and Z. Ricci (Eds.), *Critical Care Nephrology (Third Edition)* (pp. 417–423.e2). Elsevier. https://doi.org/10.1016/B978-0-323-44942-7.00071-6

Danish, M. S. S., Bhattacharya, A., Stepanova, D., Mikhaylov, A., Grilli, M. L., Khosravy, M. and Senjyu, T. (2020). A Systematic Review of Metal Oxide Applications for Energy and Environmental Sustainability. *Metals*, 10(12), Article 12. https://doi.org/10.3390/met10121604

Dmitrenko, M., Atta, R., Zolotarev, A., Kuzminova, A., Ermakov, S. and Penkova, A. (2022). Development of Novel Membranes Based on Polyvinyl Alcohol Modified by Pluronic F127 for Pervaporation Dehydration of Isopropanol. *Sustainability*, *14*(6), Article 6. https://doi.org/10.3390/su14063561

Einaga, H., Futamura, S. and Ibusuki, T. (2002). Heterogeneous photocatalytic oxidation of benzene, toluene, cyclohexene and cyclohexane in humidified air: Comparison of decomposition behavior on photoirradiated TiO2 catalyst. *Applied Catalysis B: Environmental*, *38*(3), 215–225. https://doi.org/10.1016/S0926-3373(02)00056-5

Enesca, A. and Cazan, C. (2020). Volatile organic compounds (VOCs) Removal from indoor air by Heterostructures/Composites/Doped Photocatalysts: A Mini-Review. *Nanomaterials*, 10(10), Article 10. https://doi.org/10.3390/nano10101965

Gao, M., Mao, M., Shi, J., Liu, Y., Chen, Q. and Li, J. (2023). A review of the treatment techniques of VOC. *Applied Mathematics and Nonlinear Sciences*, *8*(1), 2063–2074. https://doi.org/10.2478/amns.2021.2.00131

Guo, M., Ma, P., Wang, J., Xu, H., Zheng, K., Cheng, D., Liu, Y., Guo, G., Dai, H., Duan, E. and Deng, J. (2022). Synergy in Au–CuO janus structure for catalytic isopropanol oxidative dehydrogenation to acetone. *Angewandte Chemie International Edition*, 61(27), e202203827. https://doi.org/10.1002/anie.202203827

Hu, G., Yang, J., Duan, X., Farnood, R., Yang, C., Yang, J., Liu, W. and Liu, Q. (2021). Recent developments and challenges in zeolite-based composite photocatalysts for environmental applications. *Chemical Engineering Journal*, 417, 129209. https://doi.org/10.1016/j.cej.2021.129209

Jaison, A., Mohan, A. and Lee, Y.-C. (2023). Recent developments in photocatalytic nanotechnology for purifying air polluted with volatile organic compounds: effect of operating parameters and catalyst deactivation. *Catalysts*, *13*(2), Article 2. https://doi.org/10.3390/catal13020407

Kamegawa, T., Kido, R., Yamahana, D. and Yamashita, H. (2013). Design of TiO2-zeolite composites with enhanced photocatalytic performances under irradiation of UV and visible light. *Microporous and Mesoporous Materials*, 165, 142–147. https://doi.org/10.1016/j.micromeso.2012.08.013

Krishna, K. G., Parne, S. R. and Nagaraju, P. (2024). ZnO/CdO island-like porous nanocomposite as an ultra-sensitive sensor for BTX detection at room temperature. *Surfaces and Interfaces*, 44, 103631. https://doi.org/10.1016/j.surfin.2023.103631

Liu, W., Liu, W., Zhao, B., Zhao, L., Li, D., Fang, P. and Liu, W. (2019). Novel insights into the adsorption mechanism of the isopropanol amine collector on magnesite ore: A combined experimental and theoretical computational study. *Powder Technology*, 343, 366–374. https://doi.org/10.1016/j.powtec.2018.11.063

Mabate, T. P., Maqunga, N. P., Ntshibongo, S., Maumela, M. and Bingwa, N. (2023). Metal oxides and their roles in heterogeneous catalysis: Special emphasis on synthesis protocols, intrinsic properties, and their influence in transfer hydrogenation reactions. *SN Applied Sciences*, 5(7), 196. https://doi.org/10.1007/s42452-023-05416-6

Mo, J., Zhang, Y., Xu, Q., Lamson, J. J. and Zhao, R. (2009). Photocatalytic purification of volatile organic compounds in

indoor air: A literature review. *Atmospheric Environment*, 43(14), 2229–2246. https://doi.org/10.1016/j.atmosenv.2009.01.034

Mohammed, A. S., Kafi, D. K., Ramizy, A., Abdulhadi, O. O. and Hasan, S. F. (n.d.). *Nanocrystalline Ce-Doped CdO Thin Films Synthesis By Spray Pyrolysis Method For Solar Cells Applications*.

Moshoeshoe, M., Nadiye-Tabbiruka, M. S. and Obuseng, V. (2017). A review of the chemistry, structure, properties and applications of zeolites. *American Journal of Materials Science*, 7(5), 196–221.

Nhan, N. V. H., Tu, L. N. Q., Loc, B. T., Vinh, D. C., Phuong, N. T. T., Duong, N. T. H. and Long, N. Q. (2024). Microwave-assisted synthesis of carbon nanodots/TiO2 composite with enhanced photocatalytic oxidation of VOCs in a continuous Flow reaction. *Topics in Catalysis*, 67(9), 661–669.

Ong, W.-J., Tan, L.-L., Chai, S.-P., Yong, S.-T. and Mohamed, A. R. (2014). Facet-dependent photocatalytic properties of TiO2-based composites for energy conversion and environmental remediation. *ChemSusChem*, 7(3), 690–719. https://doi.org/10.1002/cssc.201300924

Rajput, J. K., Pathak, T. K., Kumar, V., Swart, H. C. and Purohit, L. P. (2018). Tailoring and optimization of optical properties of CdO thin films for gas sensing applications. *Physica B: Condensed Matter*, 535, 314–318. https://doi.org/10.1016/j.physb.2017.08.014

Rana, V. S., Rajput, J. K., Pathak, T. K. and Purohit, L. P. (2019). Cu sputtered Cu/ZnO Schottky diodes on fluorine doped tin oxide substrate for optoelectronic applications. *Thin Solid Films*, 679, 79–85. https://doi.org/10.1016/j.tsf.2019.04.019

Robson, H. (2001). *Verified Synthesis of Zeolitic Materials: Second Edition*. Gulf Professional Publishing.

Sharma, P., Song, J.-S., Han, M. H. and Cho, C.-H. (2016). GIS-NaP1 zeolite microspheres as potential water adsorption material: Influence of initial silica concentration on adsorptive and physical/topological properties. *Scientific Reports*, 6(1), 22734. https://doi.org/10.1038/srep22734

Tan, J., Wang, X., Hou, W., Zhang, X., Liu, L., Ye, J. and Wang, D. (2019). Fabrication of Fe3O4@graphene/TiO2 nanohybrid with enhanced photocatalytic activity for isopropanol degradation. *Journal of Alloys and Compounds*, 792, 918–927. https://doi.org/10.1016/j.jallcom.2019.03.378

Tu, L. N. Q., Nhan, N. V. H., Van Dung, N., An, N. T. and Long, N. Q. (2019). Enhanced photocatalytic performance and moisture tolerance of nano-sized Me/TiO2–zeolite Y (Me=Au, Pd) for gaseous toluene removal: Activity and mechanistic investigation. *Journal of Nanoparticle Research*, 21(9), 194. https://doi.org/10.1007/s11051-019-4642-y

Veerapandian K. P., De Geyter S., Giraudon N., Lamonier J.-M, J.-F. and Morent, R. (2019). The use of Zeolites for VOCs abatement by combining non-thermal plasma, adsorption, and/or catalysis: a review. *Catalysts*, *9*(1), Article 1. https://doi.org/10.3390/catal9010098

Wang, J. and Guo, X. (2020). Adsorption kinetic models: Physical meanings, applications, and solving methods. Journal of Hazardous Materials, 390, 122156. https://doi.org/10.1016/j.jhazmat.2020.122156

Wiegand, T. J. (2024). Isopropanol. In P. J. Wexler (Ed.), *Encyclopedia of Toxicology (Fourth Edition)* (pp. 719–723). Academic Press. https://doi.org/10.1016/B978-0-12-824315-2.00993-3

Wu, S., Ishisone, K., Sheng, Y., Manuputty, M. Y., Kraft, M. and Xu, R. (2021). TiO_2 with controllable oxygen vacancies for efficient isopropanol degradation: Photoactivity and reaction mechanism. *Catalysis Science & Technology*, 11(12), 4060–4071. https://doi.org/10.1039/D1CY00417D

Yan, X., Li, Y. and Xia, T. (2017). Black titanium dioxide nanomaterials in photocatalysis. *International Journal of Photoenergy*, 2017(1), 8529851. https://doi.org/10.1155/2017/8529851

Yan, Y., Han, M., Konkin, A., Koppe, T., Wang, D., Andreu, T., Chen, G., Vetter, U., Morante, J. R. and Schaaf, P. (2014). Slightly hydrogenated TiO2 with enhanced photocatalytic performance. *Journal of Materials Chemistry A*, *2*(32), 12708–12716. https://doi.org/10.1039/C4TA02192D

Zhang, G., Song, A., Duan, Y. and Zheng, S. (2018). Enhanced photocatalytic activity of TiO2/zeolite composite for abatement of pollutants. *Microporous and Mesoporous Materials*, 255, 61–68. https://doi.org/10.1016/j.micromeso.2017.07.028

Zhang, J. (2019). Physical insights into kinetic models of adsorption. *Separation and Purification Technology*, 229, 115832. https://doi.org/10.1016/j.seppur.2019.115832